


# Universality class of a displacive structural phase transition in two dimensions

Richard L. C. Vink

*Institute of Materials Physics, University of Goettingen, Friedrich-Hund-Platz 1, 37077 Goettingen, Germany*

 (Received 27 August 2018; revised manuscript received 6 November 2018; published 6 December 2018)

The displacive structural phase transition in a two-dimensional model solid due to Benassi *et al.* [A. Benassi *et al.*, *Phys. Rev. Lett.* **106**, 256102 (2011)] is analyzed using Monte Carlo simulations and finite-size scaling. The model is shown to be a member of the two-dimensional six-state clock model universality class. Consequently, the model features two phase transitions, implying the existence of three thermodynamically distinct phases, namely, a low-temperature phase with long-range order, an intermediate critical phase with power-law decay of correlations, and a high-temperature phase with short-range order.

DOI: [10.1103/PhysRevE.98.062109](https://doi.org/10.1103/PhysRevE.98.062109)

## I. INTRODUCTION

Complex oxide solids are known to exhibit structural phase transitions [1]. These transitions are relevant for applications, as material properties below and above the transition typically differ, but are also interesting in their own right, regarding the fundamentals of solid phase behavior. Consequently, these transitions have received considerable attention, including increasingly by means of computer simulation. An example is the study of Ref. [2], where a simple particle model is proposed featuring a displacive structural phase transition. We will, in what follows, refer to this model as the Benassi-Vanossi-Santoro-Tosatti (BVST) model and focus exclusively on its *equilibrium* phase behavior.

Despite the apparent simplicity of the BVST model, its equilibrium phase behavior is far from trivial. Indeed, the authors already announce the possibility of a Kosterlitz-Thouless (KT) transition, citing Ref. [3]. Further inspection of Ref. [3] suggests that the BVST model could be in the universality class of the two-dimensional  $q = 6$  clock model. If this is the case, the model should in fact undergo two separate phase transitions and consequently support three thermodynamically distinct phases [3]. The purpose of the present paper is to verify, via Monte Carlo (MC) simulations and finite-size scaling, whether this scenario applies.

As it turns out, our simulations strikingly show that the BVST model is a member of the  $q = 6$  clock model universality class. The existence of two phase transitions, implying three phases, is clearly visible. In addition, critical exponents obtained using finite-size scaling are consistent with those of the  $q = 6$  clock model. In what follows we will present the analysis leading to these results. The outline is as follows. We describe the BVST model [2] in Sec. II A, followed by a brief summary of the  $q = 6$  state clock model in Sec. II B. We then present our MC data in Sec. III, followed, in Sec. IV, by a discussion and summary. The details of the MC methods used in this work are provided in the Appendix.

## II. MODELS

### A. The BVST model

The BVST model [2] provides a simple description of a material exhibiting a structural phase transition. It qualitatively resembles a system whereby, during the transition, one of the particle species remains fixed (as do, e.g., Ba atoms in the case of BaTiO<sub>3</sub> [1]). The fixed species is assumed to provide an underlying lattice structure as well as to give rise to a (static) external field acting on the mobile species. It is assumed there is only one type of mobile particle species, and the total number of these particles is denoted by  $N$ . In addition, there is a pair interaction between the mobile species, described in the form of permanent anharmonic bonds. The total energy of the system is thus given by  $E = \sum_{[ij]} u_{ij} + \sum_{i=1}^N h_i$ , where  $[ij]$  is a sum over bonded pairs of particles  $i$  and  $j$ ,  $u_{ij}$  is the corresponding bond energy, and  $h_i$  is the external field acting on particle  $i$ .

The underlying crystal structure is assumed to be a hexagonal lattice, i.e., the model is purely two dimensional. The nearest-neighbor distance between lattice points is denoted by  $a$ . To each lattice position  $\vec{R}_i$ , a single particle is assigned ( $i = 1, \dots, N$ ). The displacement of particle  $i$  from its lattice position  $\vec{R}_i$  is defined as  $\vec{r}_i = (x_i, y_i)$ . During the simulations, the particle displacements  $\vec{r}_i$  are allowed to fluctuate, but the lattice positions  $\vec{R}_i$  remain fixed.

Each particle is bonded to its six nearest neighbors by means of an anharmonic spring. The spring energy is given by  $u_{ij} = b_2(d_{ij} - a)^2 + b_4(d_{ij} - a)^4$ , with  $d_{ij} = |\vec{R}_j + \vec{r}_j - \vec{R}_i - \vec{r}_i|$  the distance between the two particles. The bonds ( $3N$  in total) are assigned once at the start of the simulation. During the simulations, there is no breaking of bonds or the formation of new bonds.

The external field acting on particle  $i$  is defined in terms of its displacement  $\vec{r}_i$  as

$$\frac{h_i}{\epsilon} = 1 + \left(\frac{r_i}{a_0}\right)^4 - 2 \left[ (3 \cos \theta_i - 4 \cos^3 \theta_i) \frac{r_i}{a_0} \right]^2,$$

with  $r_i = \sqrt{x_i^2 + y_i^2}$  and  $\cos\theta_i = x_i/r_i$ . Due to the external field  $h_i$ , each lattice position  $\vec{R}_i$  is surrounded by six local energy minima, at coordinates  $\vec{R}_i + a_0(\cos\pi\lambda/3, \sin\pi\lambda/3)$ , with  $\lambda = 1, 2, 3, 4, 5, 6$ . A single particle can thus minimize its field energy by selecting one of the surrounding minima. In order to simultaneously minimize the bond energy additionally requires that all particles choose the same  $\lambda$ , which leads to the ground state of the model, where the total energy  $E = 0$ . Hence, upon lowering the temperature, one expects ordering to occur, whereby the particles collectively choose the same value of  $\lambda$ , reminiscent of a displacive structural phase transition. As will be shown later, the transition to the ordered (low-temperature) state proceeds via two phase transitions.

In what follows  $b_2 = 28.32U/a^2$ ,  $b_4 = 784.35U/a^4$ ,  $\epsilon = 0.2U$ , and  $a_0/a = 0.05$ , which are the values of Ref. [2]. The lattice constant  $a$  will be our unit of length, and temperature will be expressed in units of  $U/k_B$ , with  $k_B$  the Boltzmann constant. We use rectangular  $L_x \times L_y$  simulation cells with periodic boundary conditions in both dimensions. To prepare the initial hexagonal lattice, we take as the unit cell an  $l_x \times l_y$  rectangle, with  $l_x = a$  and  $l_y = \sqrt{3}a$ . The unit cell contains two lattice sites, at coordinates  $(0,0)$  and  $(l_x/2, l_y/2)$ . This unit cell is then replicated  $2n$  times in the  $x$  direction and  $n$  times in the  $y$  direction, with integer  $n$ . Consequently,  $N = 4n^2$ ,  $L_x = 2an$ , and  $L_y = \sqrt{3}an$  and it is ensured that, irrespective of  $n$ , all our simulation cells have the same aspect ratio  $L_x/L_y$ .

### B. The $q = 6$ clock model

The (two-dimensional)  $q$ -state clock model considers a two-dimensional space lattice (e.g., square or hexagonal) of sites  $i = 1, \dots, N$ . To each lattice site  $i$ , a discretized direction is attached, expressed via the angle  $\theta_i = 2\pi n_i/q$ , with integer  $n_i = 1, \dots, q$ . The energy  $E = -J \sum_{\langle ij \rangle} \cos(\theta_i - \theta_j)$ , the coupling parameter  $J > 0$ , and the sum is over pairs of nearest neighbors. The case  $q = 2$  is the Ising model;  $q \rightarrow \infty$  is the  $XY$  model. For  $q = 6$ , the clock model features two phase transitions [3], at temperatures  $T_1$  and  $T_2$ , respectively (we set  $T_1 < T_2$  in what follows). The model thus supports three, thermodynamically distinct, phases. The phases are characterized by the decay of the angular correlation function  $G(r) = \langle \sum_{r_{ij}=r} \cos(\theta_i - \theta_j) \rangle / N_r$ , where the sum is over all pairs of sites  $i - j$  separated by a distance  $r_{ij} = r$ ,  $N_r$  is the number of such pairs, and  $\langle \cdot \rangle$  is a thermal average.

In the high-temperature phase  $T > T_2$ , the correlations decay exponentially to zero,  $G(r) \propto e^{-r/\xi}$ ,  $\xi$  being the correlation length. The phase is disordered: There is no alignment of the angular directions over distances beyond  $\sim \xi$ , implying that the order parameter  $\Delta = 0$ . Provided the simulation box dimensions  $L_x, L_y > \xi$ , one expects only negligible finite-size effects in simulation data.

In the low-temperature phase  $T < T_1$ , there is long-range order, with a macroscopic fraction of the site orientations pointing in the same direction (which can be any one of the  $q$  possibilities). Consequently, the order parameter  $\Delta > 0$ . The correlation function still decays exponentially, but to a finite value  $G(r) - G_\infty \propto e^{-r/\xi}$ , with  $G_\infty > 0$ . Provided  $L_x, L_y > \xi$ , finite-size effects in simulation data are again negligible.

The intermediate phase  $T_1 < T < T_2$  is a critical phase, where the correlations decay as a power law  $G(r) \propto r^{-\eta}$ , implying that  $\xi$  is infinite. Power-law decay of correlations also implies that, in the thermodynamic limit, the susceptibility  $\chi$  is infinite and the order parameter  $\Delta = 0$ . Since  $L_x, L_y \ll \xi$  is now unavoidable, finite-size effects in simulation data are strong.

We emphasize that the correlation length  $\xi$ , the plateau value  $G_\infty$ , and the exponent  $\eta$  are functions of temperature. According to theoretical predictions,  $\eta(T_2) \equiv \eta_2 = 1/4$  and  $\eta(T_1) \equiv \eta_1 = 4/q^2 = 1/9$  [3]. Simulation estimates [4,5] are close to these values, though not in perfect agreement.

The consensus is (but do note discussions in Refs. [6–8]) that both transitions are of the KT type [9,10], implying exponential growth of  $\xi$  upon approach of the critical phase:

$$\xi(T) \propto \begin{cases} e^{a_1 t_1^{-1/2}}, & t_1 \equiv \frac{T_1 - T}{T_1}, \quad 0 < t_1 \ll 1 \\ \infty, & T_1 \leq T \leq T_2 \\ e^{a_2 t_2^{-1/2}}, & t_2 \equiv \frac{T - T_2}{T_2}, \quad 0 < t_2 \ll 1. \end{cases} \quad (1)$$

For the  $XY$  model at finite temperature, only the transition at  $T_2$  remains, for which  $a_{XY} \sim 1.5$  [10]. Computer simulations [4] show that this value is compatible with the  $q = 6$  clock model as well, for *both* transitions:  $a_1 = a_2 \sim 1.54$ .

The specific heat  $c_V$  of the  $q = 6$  clock model always remains finite. However, the variation of  $c_V$  with temperature does reveal two maxima, one occurring close to  $T_1$ , the other closer to  $T_2$ . This property is convenient in simulations to provide early evidence of two phase transitions [4].

## III. RESULTS

In what follows, moderate system sizes  $L \equiv L_x = 30\text{--}80$  are used to study the BVST model (see the Appendix for details about the MC methods). This approach is in line with Ref. [11], where it was noted that moderate system sizes, in combination with finite-size scaling methods, can yield a very adequate description of the phase behavior in the thermodynamic limit.

### A. Specific heat

In Fig. 1 we plot the specific heat per particle of the BVST model,  $c_V = (\langle E^2 \rangle - \langle E \rangle^2) / NT^2$ , versus the temperature  $T$ , for various system sizes  $L$ . Consistent with the  $q = 6$  clock model, the data strikingly reveal two maxima, corresponding to two phase transitions. In addition, finite-size effects in  $c_V$  are small. The absence of a strong increase of the peak heights with  $L$  indicates that  $c_V$  does not diverge at any of the transitions, consistent with the  $q = 6$  clock model. The reader is encouraged to compare our Fig. 1 to specific-heat MC data of the  $q = 6$  clock model [4,12], which look very similar.

### B. Susceptibility

For a given set of particle displacements, in line with Ref. [2], we use the vector sum  $M = |\sum_{i=1}^N \vec{r}_i|/a_0$  to quantify the degree of order. In the perfectly ordered ground state  $M/N = 1$ , since here all the particles have selected the same minimum, while  $M/N < 1$  when the ordering is not perfect.

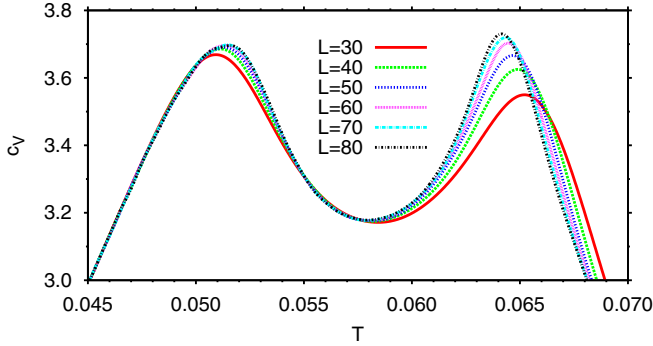


FIG. 1. Specific heat  $c_V$  of the BVST model versus the temperature  $T$  for various system sizes  $L$ . The data reveal two maxima, consistent with the two-transition scenario of the  $q = 6$  clock model. Note that finite-size effects in the peak heights are weak, indicating that  $c_V$  does not diverge at any of the transitions.

In the language of vector spin models,  $M$  is analogous to the absolute value of the total magnetization, commonly used in studies of the  $q = 6$  clock model [4,12]. Note, however, that this is not the only possible choice; for example, an angular order parameter could be used also [13]. We now define the susceptibility  $\chi = (\langle M^2 \rangle - \langle M \rangle^2)/NT$ , which we plot in Fig. 2 as a function of temperature, for various system sizes. The key observations are that finite-size effects are negligible in the low- and high-temperature regimes, while they are very strong in the intermediate regime, roughly corresponding to the temperature range spanned by the specific-heat maxima. The pronounced increase of  $\chi$  with  $L$  at intermediate temperatures is consistent with a critical phase, where  $\chi \rightarrow \infty$  in the thermodynamic limit  $L \rightarrow \infty$ . Hence, Fig. 2 supports the two-transition scenario of the  $q = 6$  clock model, with noncritical phases at low and high temperature, separated by a critical phase (although we still need to check the nature of the order in each of the phases).

### C. Phase transition temperatures

To determine the transition temperatures, we perform a finite-size scaling analysis. In a system of size  $L$ , approaching

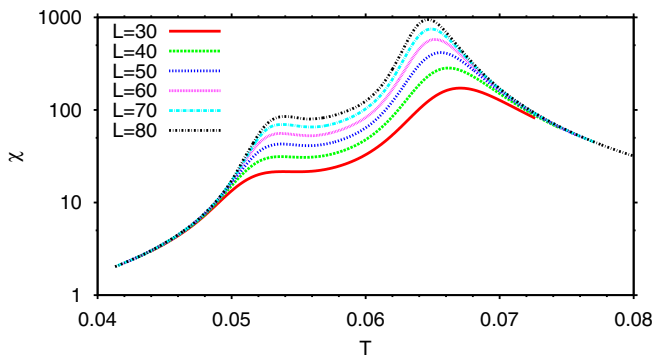


FIG. 2. Susceptibility  $\chi$  of the BVST model versus the temperature  $T$  for various system sizes  $L$ . The data reveal negligible size effects at low and high temperature, while  $\chi$  increases strongly with  $L$  at intermediate temperatures (note the vertical logarithmic scale). This supports the two-transition scenario of the  $q = 6$  clock model.

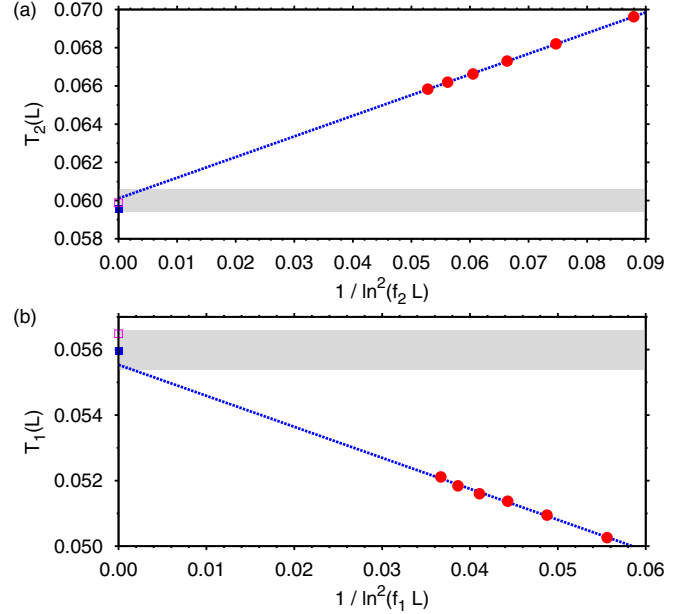


FIG. 3. Finite-size scaling analysis of the temperatures (a)  $T_2(L)$  and (b)  $T_1(L)$ , assuming the transitions are of the KT type. The intercept of the lines yields the transition temperature of the thermodynamic limit when all three parameters are fitted. The squares indicate the transition temperature obtained for two-parameter fits, where  $a_1 = a_2 = a_{XY}$  was imposed, using all system sizes (closed squares) and system sizes  $L = 70, 80$  (open squares).

the lower transition at  $T_1$  from below, Fig. 2 shows that the slope  $d\chi/dT$  initially increases and then levels off, i.e.,  $d\chi/dT$  reaches a local maximum. Let  $T_1(L)$  be the temperature at the maximum. Similarly, approaching the upper transition at  $T_2$  from above,  $d\chi/dT$  reaches a local minimum, defining  $T_2(L)$ . In the limit  $L \rightarrow \infty$ , these finite-size estimators converge to the transition temperature of the thermodynamic limit:  $\lim_{L \rightarrow \infty} T_i(L) = T_i$  ( $i = 1, 2$ ).

Assuming the  $q = 6$  clock model scenario, the transitions at  $T_1$  and  $T_2$  are both of the KT type, with  $\xi$  given by Eq. (1). This implies scaling relations  $T_1(L) = T_1 - a_1^2/\ln^2(f_1 L)$  and  $T_2(L) = T_2 + a_2^2/\ln^2(f_2 L)$ , with  $f_i$  constants of order unity and  $a_i$  the coefficients of Eq. (1) [14]. In Fig. 3(a) we fit our  $T_2(L)$  estimates to the expected scaling form. The fit captures the data well, using  $T_2 \approx 0.060$ ,  $a_2 \approx 1.3$ , and  $f_2 \approx 1.0$ . Figure 3(b) shows the corresponding fit to our  $T_1(L)$  data, where  $T_1 \approx 0.056$ ,  $a_1 \approx 1.3$ , and  $f_1 \approx 2.3$  yielded the best fit. It is gratifying that both fits yield the same value for  $a_i$ , although the expected KT value is somewhat higher. If we repeat the procedure setting  $a_1 = a_2 = a_{XY} \sim 1.5$  and only fit  $f_i$  and  $T_i$ , we obtain good fits also. The closed squares in Fig. 3 indicate the transition temperatures obtained in this way, with  $f_1 \approx 3.7$  and  $f_2 \approx 1.3$ . Finally, again setting  $a_1 = a_2 = a_{XY} \sim 1.5$ , but this time only using data for  $L = 70, 80$ , i.e., our largest systems, the open squares are obtained. From this analysis, we conclude that  $T_1 = 0.0560 \pm 0.0006$ , and  $T_2 = 0.0600 \pm 0.0006$ ; the vertical height of the shaded bands in Fig. 3 indicates the corresponding ranges.

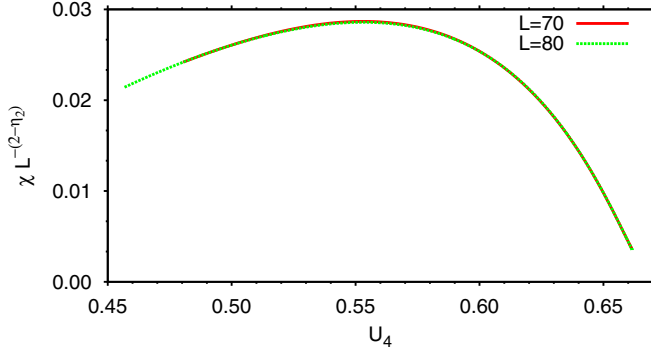


FIG. 4. Application of the method of Loison [15] to obtain the critical exponent  $\eta_2$  of the high-temperature transition. For this analysis, only data in the high-temperature phase,  $0 < t_2 < 0.1$ , were used, with  $t_2$  defined in Eq. (1). Substituting the accepted value  $\eta_2 = 1/4$ , an excellent collapse of the data is observed.

#### D. Critical exponents

Next we turn to measuring the critical exponent  $\eta_2$ , i.e., the value of  $\eta$  at the high-temperature transition. The latter is most conveniently obtained using the method of Loison [15]; see also Ref. [13], where this method is applied to the  $q = 8$  clock model. Here one varies  $T$  and plots the scaled susceptibility  $\chi L^{-(d-\eta_2)}$ , with  $d = 2$  the spatial dimension, as a function of the Binder cumulant  $U_4 = 1 - \langle M^4 \rangle / 3 \langle M^2 \rangle^2$ . Provided the correct value of  $\eta_2$  is used, the data for different system sizes  $L$  should collapse onto a single curve. The result is shown in Fig. 4, where the accepted value  $\eta_2 = 1/4$  was substituted, using our largest set of system sizes  $L = 70, 80$ . The quality of the collapse is quite remarkable. If we repeat the analysis using all our available system sizes, a somewhat larger exponent  $\eta_2 \sim 0.3$  is obtained. In Ref. [13], it is mentioned that deviations are likely due to logarithmic size corrections, which still are strong in small system sizes. Hence, we believe that  $\eta_2 = 1/4$  obtained for our largest systems is the most reliable estimate, fully consistent with the  $q = 6$  clock model.

For the low-temperature transition, Loison's method is not directly applicable and so to obtain  $\eta_1$ , we follow a different route, based on the order parameter  $\Delta = \langle M \rangle / N$ . In the critical intermediate phase, i.e., for temperatures  $T_1 \leq T \leq T_2$ , the order parameter vanishes, following finite-size scaling, as  $\Delta \propto L^{-\eta(T)/2}$ , where the exponent  $\eta(T)$  is an increasing function of  $T$ . For  $T < T_1$ , i.e., in the ordered phase,  $\Delta$  is finite, since here there is long-range order. Consider now the quantity  $\Delta L^{\eta_1/2}$ , with  $\eta_1 = 1/9$  being the expected theoretical value of  $\eta(T)$  at the lower transition temperature  $T_1$ . This quantity should diverge with  $L$  for  $T < T_1$  (since here  $\Delta$  is finite), remain constant at  $T_1$ , and decay to zero above  $T_1$  [since  $\eta(T)$  increases with  $T$ ]. Hence, plotting  $\Delta L^{\eta_1/2}$  versus  $T$ , for different system sizes  $L$ , the data for different  $L$  are expected to intersect at  $T = T_1$ . The result is shown in Fig. 5(a), which clearly reveals intersections. For a pair of system sizes  $(L_i, L_j)$ , we now define  $T_X$  as the temperature where the corresponding curves intersect. Figure 5(b) shows  $T_X$  versus  $1/\ln^2(L^*)$ ,  $L^* \equiv (L_i + L_j)/2$ , for all available pairs ( $L = 30, 40, 50, 60, 70, 80$ , i.e., a total of 15 pairs). As  $L^*$  increases, there is a clear trend for  $T_X$  to increase as well,

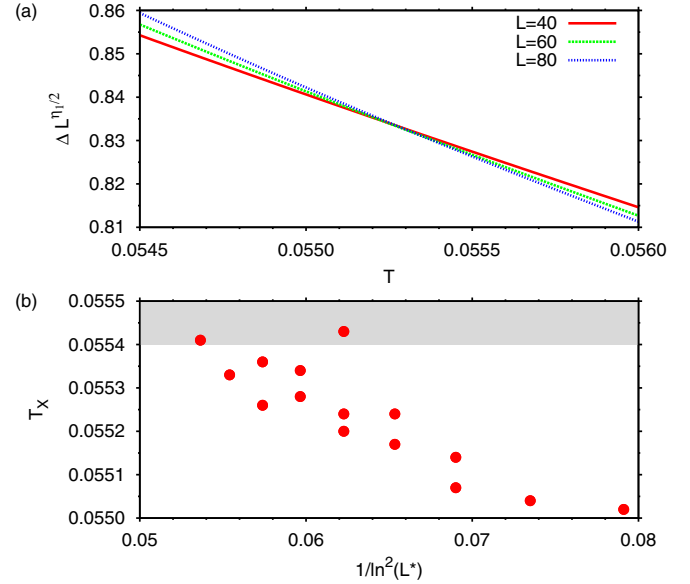


FIG. 5. Finite-size scaling analysis of the order parameter  $\Delta$  in the vicinity of the low-temperature transition. (a) Plot of  $\Delta L^{\eta_1/2}$  versus  $T$  for three different system sizes  $L$ , where  $\eta_1 = 1/9$  was used. Note that curves for different  $L$  intersect. (b) Intersection temperatures  $T_X$  for pairs of system sizes plotted versus  $1/\ln^2 L^*$ . The shaded region marks the lower portion of the  $T_1$  estimate range of Fig. 3(b). As  $L^*$  increases,  $T_X$  approaches this range.

approaching values that are consistent with Fig. 3(b). Hence, while Fig. 5 does not constitute a direct measurement of  $\eta_1$ , it does show that the BVST model is *consistent* with the theoretically expected  $q = 6$  clock model value  $\eta_1 = 1/9$ .

#### E. Correlation functions

Finally, we still present the correlation function  $G(r)$  (Fig. 6). For  $T < T_1$ , one indeed finds that  $G(r)$  decays to a finite plateau value, consistent with long-range order, and a finite correlation length  $\xi$ . For  $T > T_2$ ,  $G(r)$  quickly decays

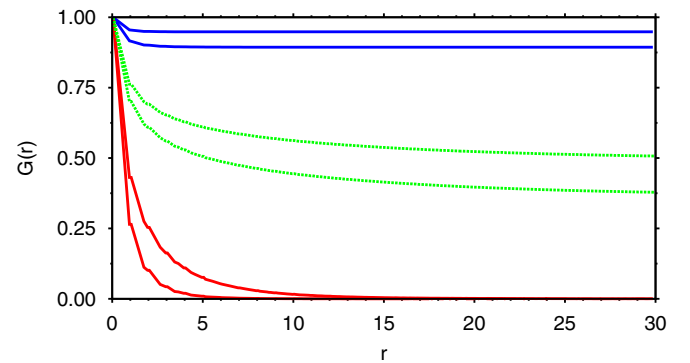


FIG. 6. Correlation functions  $G(r)$  of the BVST model obtained at  $T = 0.04, 0.045$  (top two curves),  $T = 0.056, 0.06$  (middle two curves), and  $T = 0.075, 0.1$  (bottom two curves). The three sets of curves represent, from top to bottom, the low-temperature phase with long-range order, the critical intermediate phase with power-law decay of correlations, and the high-temperature phase with short-range order.



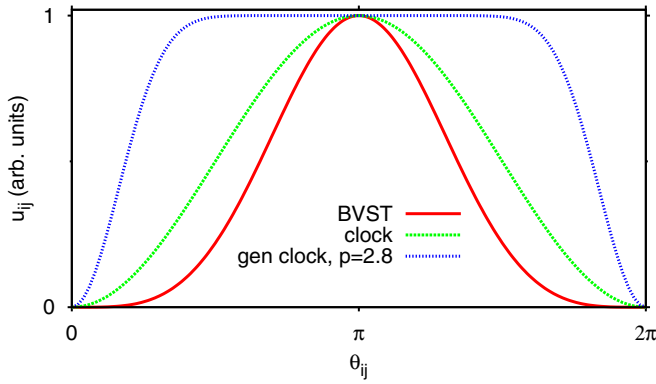


FIG. 7. Shape of the nearest-neighbor pair interaction for the BVST model, the clock model, and the generalized clock model using  $p = 2.8$ . In this plot, the potential minimum of each interaction was shifted to zero, followed by a scaling of the potential to have the maximum at unity.

to zero, consistent with short-range order, and finite  $\xi$ . In the intermediate phase,  $G(r)$  decays slowly, but there is no sign of  $G(r)$  saturating to a finite value, consistent with a critical phase where  $\xi$  is infinite. Hence, also the dependence of  $G(r)$  on temperature is consistent with the  $q = 6$  clock model.

#### IV. CONCLUSION

We have presented MC data of the BVST model, showing that it belongs to the universality class of the two-dimensional  $q = 6$  clock model. The hallmark features are the presence of two KT transitions with, consequently, three thermodynamically distinct phases. Our data are consistent with the theoretical  $q = 6$  clock model critical exponents  $\eta_1 = 1/9$  and  $\eta_2 = 1/4$ , of the lower and the higher transition, respectively. Our estimates of the transition temperatures  $T_1$  and  $T_2$  are somewhat below the  $T_c \approx 0.075$  reported in Ref. [2]. However, since the focus of Ref. [2] was on frictional behavior, no finite-size scaling study was performed, which we believe explains the deviation.

The reason the BVST model is in the  $q = 6$  clock model universality class is due to the external field  $h_i$  and the bond potential  $u_{ij}$ . For each particle, the field gives rise to six local energy minima for this particle, corresponding to the clock states. It is important to note that, already at temperatures  $T \sim T_2$ , the external field is confining each particle to its set of minima. Hence, even though each particle in the BVST model has two degrees of freedom  $\vec{r}_i = (x_i, y_i)$ , the field effectively reduces this to a set of six possible angles  $\theta_i = \pi\lambda/3$ ,  $|\vec{r}_i| = a_0$ ,  $\lambda = 1, \dots, 6$ , just as in the clock model. If we now plot the BVST bond energy  $u_{ij}$  as a function of the angular difference  $\theta_{ij}$  between two nearest-neighbor particles, the bell-shaped BVST curve of Fig. 7 is obtained, which qualitatively resembles the cosine shape of the pair potential of the clock model. Hence, in the BVST model, both the number of states and the shape of the pair potential correspond to the  $q = 6$  clock model, which explains why the universality classes are the same.

We still comment on the possibility of a single transition. Our data indicate that the difference in transition temperatures

$T_2 - T_1$  is rather small. Hence, a critical reader might argue that, in the limit  $L \rightarrow \infty$ , the two transitions could well merge into one. However, based on what is known about clock models and their generalizations, this scenario is unlikely. The above-mentioned merging of transitions is known to happen in generalized clock models, where the nearest-neighbor interaction  $u_{ij} \sim 1 - \cos^{2p}(\theta_{ij}/2)$ , which reduces to the standard clock model when  $p = 1$ . The two transitions merge into a single transition when the nearest-neighbor interaction becomes sufficiently sharp and narrow, implying a large enough value of  $p$ . For the  $q = 8$  clock model, the corresponding value  $p > 2.8$  [13]. However, as one can see in Fig. 7, the BVST pair potential is far removed from the sharp and narrow shape required to bring about such merging (on the contrary, the BVST model rather resembles  $p < 1$ ). As a side remark, if the transitions were to merge, we should expect two-dimensional  $q = 6$  state Potts behavior [13]. The latter has a first-order transition [16], for which neither our data nor that of Ref. [2] show any evidence.

Finally, we discuss what might be expected in  $d = 3$  dimensions. In  $d = 3$ , the clock model has a single second-order phase transition, for all values of  $q$  [17]. For  $q = 6$ , the critical exponents are consistent with those of the  $d = 3$ , XY model [18]. Hence, the two-transition scenario of  $d = 2$  does not survive in  $d = 3$ . We emphasize that, in the  $d = 3$  clock and XY models, only the lattice space is three dimensional; the angular degrees of freedom remain two dimensional. A more realistic description of a displacive transition in  $d = 3$  should likely use three-dimensional displacement vectors. For an fcc material, a possible generalization of the BVST model could be an fcc lattice, where, to each lattice site, 12 minima are assigned, each one displaced a small distance in the direction of one of the nearest neighbors. Such a model could easily be simulated using Monte Carlo methods, but we are not aware of such simulations having been carried out.

#### ACKNOWLEDGMENTS

The author acknowledges support from the German Research Foundation (Grant No. SFB-1073/A01) and is additionally indebted to an anonymous referee for pointing out the two-transition scenario of the six-state clock model, and its possible connection to the BVST model.

#### APPENDIX: MONTE CARLO METHODS

We simulate the BVST model using various MC techniques. The principal MC move is always the random selection of a single particle, which then gets translated by a (two-dimensional) vector drawn randomly from a circle of radius  $r/a = 0.03$ . The use of a single-particle move restricts us to moderate system sizes, owing to critical slowing down, but these nevertheless suffice to demonstrate the connection to the  $q = 6$  clock model, our main conclusion. To overcome critical slowing down, a cluster move for the BVST model is required, the development of which is beyond the scope of this work. For the determination of the correlation functions (Fig. 6), standard Metropolis sampling was used, where each MC move is accepted with probability  $P = \min[1, \exp(-\Delta E/k_B T)]$ , with  $\Delta E$  the

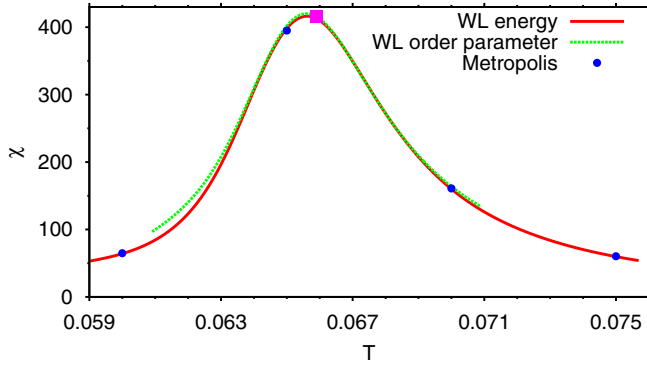


FIG. 8. Susceptibility  $\chi$  versus temperature  $T$ , for system size  $L = 50$ , obtained using three different MC methods. There is overall good agreement between WL energy sampling and the Metropolis method. For WL order parameter sampling, the simulation temperature that was used is marked with a square. In the vicinity of this temperature, there is good agreement with the other methods, but agreement deteriorates as one moves away from this temperature.

energy difference between the initial and proposed states and  $T$  the temperature. For the determination of thermodynamic quantities of interest ( $c_V$ ,  $\chi$ ,  $\Delta$ ,  $U_4$ , ...) as a function of  $T$ , we used Wang-Landau (WL) energy sampling [19,20]. In this method, the simulation performs a random walk on the energy range of interest  $0.05 < E/N < 0.17$ , chosen such that both transitions are captured (the range was discretized in steps  $\Delta E = 0.25$ ). The principal output of these simulations is the density of states  $g(E)$ . Thermal averages may then be computed for any temperature

of interest using  $\langle X \rangle = Z^{-1} \sum_E X_E g(E) e^{-E/K_B T}$ , where  $X_E$  denotes the microcanonical average of  $X$  and normalization  $Z = \sum_E g(E) e^{-E/K_B T}$ . For example, to compute energy moments  $\langle E^k \rangle$ , one sets  $X_E = E^k$ . To compute order parameter moments  $\langle M^k \rangle$ , one sets  $X_E = M_E^k$ , defined as the average value of  $M^k$  in the bin corresponding to energy  $E$ . The latter quantities are readily collected during WL sampling by updating a small number of array elements after each MC move. In locating the temperatures  $T_i(L)$  of Fig. 3, the slope  $d\chi/dT$  needs to be computed. For better accuracy, we expressed  $d\chi/dT$  in terms of appropriate moments of  $E$  and  $M$ , as opposed to using a finite-difference scheme to differentiate  $\chi$  directly (for example,  $d\langle M \rangle/dT \propto \langle ME \rangle - \langle M \rangle \langle E \rangle$ ). To further enhance efficiency, we complemented our WL simulations by the collection of transition matrix elements [21,22], following the implementation of Ref. [23]. In our simulations, the energy range of interest is split into  $\sim 15$ – $30$  intervals, with a single processor assigned to each interval (runtime per processor  $\sim 44$ – $88$  h), the data being combined afterward. The accept rate of MC moves varies  $\sim 10$ – $40$  % (highest on the high-energy side), performance being  $\sim 4 \times 10^6$  attempted moves per second. In Ref. [24], WL sampling was performed over a specified order parameter range (see also Ref. [25]). This method is advantageous for systems where reaching the ordered state is difficult, but has the disadvantage that the range in temperature over which one can reliably compute thermal averages is restricted. Since now two transitions need to be sampled, sampling over a specified energy range turned out to be the optimal choice. In Fig. 8 we present a comparison between measurements of the susceptibility obtained using all three methods.

- [1] R. A. Cowley, Structural phase transitions I. Landau theory, *Adv. Phys.* **29**, 1 (1980).
- [2] A. Benassi, A. Vanossi, G. E. Santoro, and E. Tosatti, Sliding over a Phase Transition, *Phys. Rev. Lett.* **106**, 256102 (2011).
- [3] J. V. José, L. P. Kadanoff, S. Kirkpatrick, and D. R. Nelson, Renormalization, vortices, and symmetry-breaking perturbations in the two-dimensional planar model, *Phys. Rev. B* **16**, 1217 (1977).
- [4] M. S. S. Challa and D. P. Landau, Critical behavior of the six-state clock model in two dimensions, *Phys. Rev. B* **33**, 437 (1986).
- [5] Y. Tomita and Y. Okabe, Probability-changing cluster algorithm for two-dimensional XY and clock models, *Phys. Rev. B* **65**, 184405 (2002).
- [6] C. M. Lapilli, P. Pfeifer, and C. Wexler, Universality Away from Critical Points in Two-Dimensional Phase Transitions, *Phys. Rev. Lett.* **96**, 140603 (2006).
- [7] C. O. Hwang, Six-state clock model on the square lattice: Fisher zero approach with Wang-Landau sampling, *Phys. Rev. E* **80**, 042103 (2009).
- [8] S. K. Baek, P. Minnhagen, and B. J. Kim, Comment on “Six-state clock model on the square lattice: Fisher zero approach with Wang-Landau sampling”, *Phys. Rev. E* **81**, 063101 (2010).
- [9] J. M. Kosterlitz and D. J. Thouless, Ordering, metastability and phase transitions in two-dimensional systems, *J. Phys. C* **6**, 1181 (1973).
- [10] J. M. Kosterlitz, The critical properties of the two-dimensional xy model, *J. Phys. C* **7**, 1046 (1974).
- [11] G. Orkoulas, A. Z. Panagiotopoulos, and M. E. Fisher, Criticality and crossover in accessible regimes, *Phys. Rev. E* **61**, 5930 (2000).
- [12] J. Tobochnik, Properties of the  $q$ -state clock model for  $q = 4, 5$ , and  $6$ , *Phys. Rev. B* **26**, 6201 (1982).
- [13] S. K. Baek, P. Minnhagen, and B. J. Kim, True and quasi-long-range order in the generalized  $q$ -state clock model, *Phys. Rev. E* **80**, 060101 (2009).
- [14] S. G. Chung, Essential finite-size effect in the two-dimensional XY model, *Phys. Rev. B* **60**, 11761 (1999).
- [15] D. Loison, Binder’s cumulant for the Kosterlitz-Thouless transition, *J. Phys.: Condens. Matter* **11**, L401 (1999).
- [16] F. Y. Wu, The Potts model, *Rev. Mod. Phys.* **54**, 235 (1982).
- [17] P. D. Scholten and L. J. Irakliotis, Critical behavior of the  $q$ -state clock model in three dimensions, *Phys. Rev. B* **48**, 1291 (1993).
- [18] S. Miyashita, Nature of the ordered phase and the critical properties of the three dimensional six-state clock model, *J. Phys. Soc. Jpn.* **66**, 3411 (1997).

- [19] F. Wang and D. P. Landau, Efficient, Multiple-Range Random Walk Algorithm to Calculate the Density of States, *Phys. Rev. Lett.* **86**, 2050 (2001).
- [20] F. Wang and D. P. Landau, Determining the density of states for classical statistical models: A random walk algorithm to produce a flat histogram, *Phys. Rev. E* **64**, 056101 (2001).
- [21] M. Fitzgerald, R. R. Picard, and R. N. Silver, Canonical transition probabilities for adaptive Metropolis simulation, *Europhys. Lett.* **46**, 282 (1999).
- [22] J. R. Errington, Direct calculation of liquid-vapor phase equilibria from transition matrix Monte Carlo simulation, *J. Chem. Phys.* **118**, 9915 (2003).
- [23] M. S. Shell, P. G. Debenedetti, and A. Z. Panagiotopoulos, An improved Monte Carlo method for direct calculation of the density of states, *J. Chem. Phys.* **119**, 9406 (2003).
- [24] R. L. C. Vink, Critical behavior of a displacive structural phase transition in two dimensions, [arXiv:1808.08191](https://arxiv.org/abs/1808.08191).
- [25] R. L. C. Vink, A finite-temperature Monte Carlo algorithm for network forming materials, *J. Chem. Phys.* **140**, 104509 (2014).